Reflectarray Feeds Augmented With Size-Reducing GRIN Lenses for Improved Power Handling and Aperture Efficiency

ERIC B. WHITING (Member, IEEE), **GALESTAN MACKERTICH-SENGERDY** (Member, IEEE),
RYAN J. CHAKY (Graduate Student Member, IEEE),
COLIN A. MUSSMAN (Graduate Student Member, IEEE), SAWYER D. CAMPBELL (Senior Member, IEEE),
PINGJUAN L. WERNER (Life Senior Member, IEEE), AND DOUGLAS H. WERNER (Fellow, IEEE)

Department of Electrical Engineering, The Pennsylvania State University, University Park, PA 16802, USA

CORRESPONDING AUTHOR: S. D. CAMPBELL (e-mail: sdc22@psu.edu)

ABSTRACT The feed for reflectarrays and transmitarrays is crucial for determining the overall antenna aperture efficiency, gain, and power handling. In the past, several methods, such as altering the horn shape to achieve higher modes, have been employed to modify the feed radiation pattern to improve these key parameters. However, another approach is to use gradient index (GRIN) lenses, which offer unprecedented control over the radiation pattern and can be used to shrink the overall antenna. In this paper, we demonstrate highly effective approaches for optimizing GRIN lenses to achieve different design objectives including high gain radiation with a compact feed as well as improved aperture efficiency and power handling. Additive manufacturing is employed to fabricate the lenses, and measured results agree well with simulations.

INDEX TERMS Gradient index, lens, optimization, horn antennas, reflectarrays.

I. INTRODUCTION

REFLECTARRAY and transmitarray antennas have many advantages over traditional high-gain designs, such as parabolic dishes and phased-array systems [1]. Compared to parabolic dishes, reflectarray (RA) and transmitarray (TA) antennas offer faster reconfigurable beam steering and multibeam operation. Meanwhile, compared to phased-array systems, RA and TA antennas are often simpler to construct. For these reasons, RA and TA antenna designs that achieve high aperture efficiency and handle high power levels are of significant interest for radar and long-distance communications applications.

For any aperture antenna, maximizing the aperture efficiency is highly desirable as it directly affects the tradeoff between overall footprint and realized gain; maximizing aperture efficiency can lead to considerable SWaP-C (size, weight, power, and cost) reductions for a targeted realized gain. While the overall aperture efficiency depends on many variables, the main limiting factors are illumination and spillover efficiencies [2]. Other factors include blockage by

the feed and support structures, material losses, and phase discretization effects.

The illumination efficiency is a measurement of the field amplitude uniformity across the antenna aperture, while the spillover efficiency describes the ratio of the total radiated power to that which is incident on the reflector [3]. These two factors are determined based on the shape of the reflector and the feed source. Roughly fifty years ago, considerable effort was made to develop feeds that maximized aperture efficiency [4], [5], [6]. Some of the approaches explored since then include multimode [7], [8], corrugated [9], [10], and dielectric-loaded horns [11], [12], [13], as well as homogeneous dielectric lenses [14] and array feeds. Recently, metamaterials [15] and dielectric materials [16], [17], [18], [19], [20] have been used to improve the far-field gain of horn antennas. However, these previous design studies have not considered the aperture efficiency improvement of RA antennas.

In this paper, we propose using a Gradient Index (GRIN) lens to augment a conventional horn antenna to reduce

the overall size of the reflector feed while improving the aperture efficiency of a representative planar RA antenna. GRIN lenses possess spatially varying (*i.e.*, inhomogeneous) permittivities which give them greater control over the propagation of electromagnetic waves than traditional homogeneous lenses. GRIN lenses can be fabricated using additive [21] or subtractive manufacturing [22], [23] techniques. Moreover, they can be constructed from metamaterials [15] when anisotropic behaviors and/or inhomogeneous permeabilities are required. The predominant approach for GRIN lens design is transformation optics [24], [25], which has been successfully employed to create lenses that enhance gain [26], [27], [28], [29], reduce sidelobes [18], [30], and produce multibeam emission [31], [32], [33]. Other approaches for GRIN lens design include ray-tracing [34] and the field transformation technique [27]. In this work, we combine multiple optimization approaches with full-wave simulation to design bespoke GRIN lenses for offset-fed planar square RAs. While the remainder of this paper deals only with RA antennas, the same principles also apply to TA antennas.

This paper describes two pathways for GRIN lens integration into RA systems. The first approach, examined in Section II, presents a tradeoff study of different GRIN lens designs with varying sizes and realized gain levels. A design was fabricated to demonstrate how the feed size for an RA antenna system could be reduced with a lens mounted on top of a short horn. This SWaP-reduced feed source could be useful for minimizing blockage, shrinking the reflectarray's overall dimensions, and for feeding smaller reflectors or reflectarrays where conventional horns are often quite large. The design approach discussed in Section III concerns GRIN lenses which are optimized to maximize the aperture efficiency and power handling capability of the RA. These lenses are useful for reducing system size for a targeted gain value, which can lead to fabrication cost reductions as well as a more evenly distributed incident field across the RA surface. This can increase the safety margin for operation (an important factor for high-power microwave (HPM) applications) or allow the RA to handle more power with a simultaneously reduced size.

In these studies, the GRIN lens is placed directly on and mounted to the mouth of the horn. This allows the lens to serve as a radome for the horn feeds and enables them to be pressurized. While this behavior was not pursued in this study, a simple modification of the lenses would be to introduce a dielectric shell to eliminate any air gaps and ensure pressurization of the augmented lens/horn feed system.

II. SIZE-REDUCING GRIN LENSES

In this first section, we will employ custom numerical optimization techniques to design GRIN lens augmented horn feeds to achieve similar gains as larger horns, albeit with a smaller cross-sectional area and height.
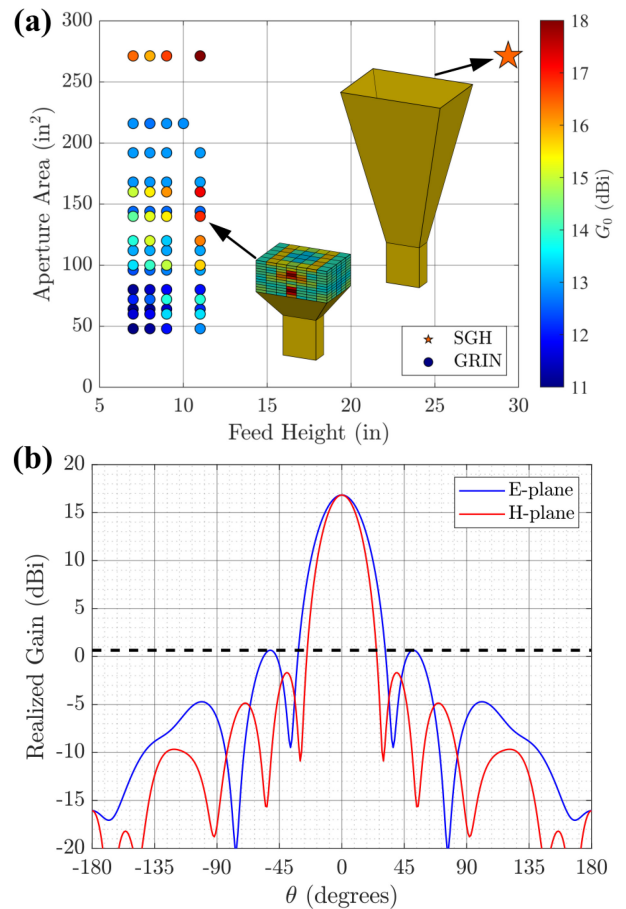

FIGURE 1. (a) A comparison of the height and aperture size of various GRIN lens feeds compared to the standard gain horn (SGH). The inset figures show the size comparison between the smallest GRIN lens design with the same gain as the SGH. (b) The simulated realized gain patterns at 1.5 GHz for the smallest GRIN lens with the same gain as the SGH.

A. OPTIMIZING LENSES WITH DIFFERENT SIZES

For large RAs, the horn size is of little consequence since it is typically small compared to the reflector. However, for smaller RAs (on the order of 10 wavelengths), utilizing a high-gain feed is still desired to achieve uniform illumination and reduce spillover. Yet, high gain horns can be quite large and cause significant blockage. To mitigate these detrimental effects, we explored reducing the cross-sectional area of the GRIN and minimizing the feed's overall height.

Previously, an adjoint sensitivity method was developed to design GRIN lenses with a similar aperture size as a 20 dB standard gain horn, albeit with reduced total height [16]. Using this approach, various-sized GRIN lenses were optimized for maximum broadside gain. However, unlike in the previous study, which only sought to reduce the overall height, here we desired to shrink the aperture dimensions as well. Figure 1(a) shows the set of lenses optimized for maximum gain but with a significantly reduced size. Each lens design represented by a circle in Figure 1(a) has a different cross-sectional width, length, and thickness. The feed horn for the lens was fixed at 5 in (127 mm) tall
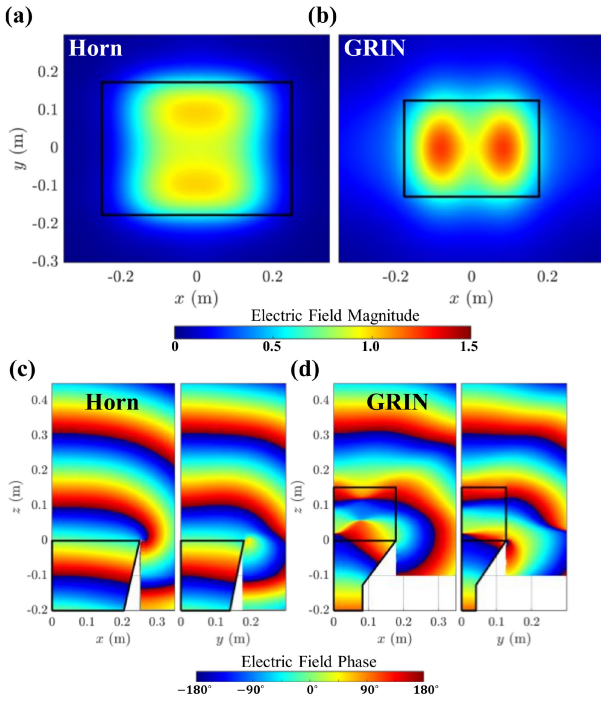
FIGURE 2. The magnitude of the electric field 5 cm above the (a) standard gain horn (SGH) and (b) the GRIN lens as shown in Figure 1. The (left) xz- and (right) yz-plane electric phase cuts for the (c) SGH and (d) the short horn with the GRIN lens.
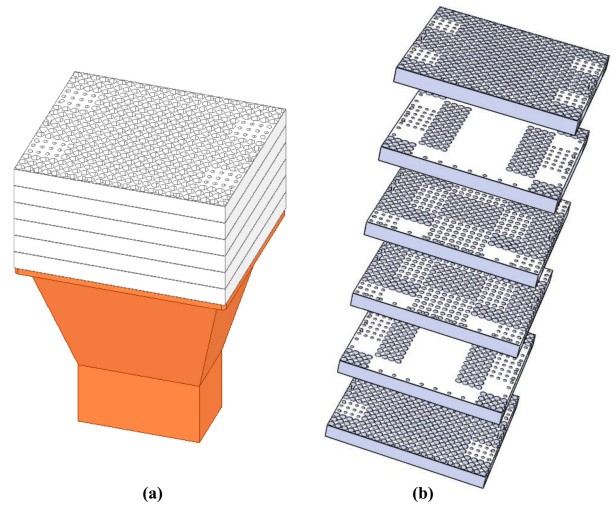

FIGURE 3. (a) The GRIN lens simulated as discrete layers with varying hole sizes to modify the permittivity. (b) Exploded CAD view demonstrating the mirroring of the three dielectric slabs, as well as the two-fold symmetry within each dielectric slab.

and had the same aperture dimensions as the GRIN lens. The permittivity was allowed to vary between 1 and 10 for each discrete block that made up the lens. The blocks were 2 x 2 x 0.5 in^3 (50.8 x 50.8 x 12.7 mm^3) with the intention that the designs could be realized using Preperm 3D printer materials [35]. Unsurprisingly, larger feeds generally do better than smaller ones. However, all solutions are much smaller than the standard gain horn (SGH). The inset shows the SGH for comparison and the best GRIN lens that achieves similar gain as the SGH. This GRIN lens design is 6 in (152.4 mm) thick and has an aperture size of 14 x 10 in^2 (355.6 x 254 mm^2). The SGH has an aperture size of 19.7 x 13.8 in^2 (500.38 x 350.52 mm^2) and a height of 29.4 in (746.76 mm). The relative permittivity of each block is between 2 and 5.1, with most dielectric blocks having a relative permittivity of less than 3. Figure 1(b) shows the simulated (COMSOL Multiphysics v5.6) realized gain for the best GRIN lens. The peak gain is around 16.9 dBi, which is comparable to that of the SGH. This design also possesses a peak side lobe level of 0.7 dB, lower than that of the SGH (see Figure 5(a)).

This design demonstrates that we can significantly reduce the overall size of the feed horn and therefore reduce the associated blockage for a RA system. In addition, we reduced the side lobe levels, which should result in lower spillover. The effective aperture area is 240 in^2 (0.155 m^2), which is much greater than the physical cross-sectional area of 140 in^2 (0.090 m^2). Figures 2(a) and (b) show the electric field magnitude 5 cm above the SGH aperture and the GRIN lens, respectively. The SGH has most of the field

concentrated in the center of the horn as would be expected for the TE$_{10}$ mode of operation. By comparison, the GRIN lens more evenly distributes the electromagnetic wave across the smaller aperture. Figures 2(c) and (d) show the phase of the electric field in both the *xz-* and *yz*-planes for the SGH and the GRIN lens, respectively. For the SGH, the phase contours are flat in both planes directly above the horn aperture and include some mild wavefront curvature towards the edges. In contrast, the GRIN lens design has planar wavefronts directly above the GRIN lens and in the regions beyond the edges of the lens. The radiation from the sides of the lens helps to spread out the electric field and create a larger effective area where the wavefront is planar. In some ways, the proposed GRIN lens is similar to both a conventional lens and a dielectric rod antenna (*e.g.*, [36]) with radiation coming from both the front and sides of the lens, yet it is much narrower than a conventional lens while also being much shorter than a dielectric rod antenna. In the next section, we realize a compact feed with a lens and horn optimized for a chosen fabrication method.

B. FABRICATED LENS DESIGN
Several modifications were implemented into the GRIN setup to make the lens fabrication easier and more robust, after which the lens was reoptimized in HFSS. The first modification was to choose a commercially available horn with dimensions of 10.75 x 9.05 x 8.7 in^3 (273.05 x 229.87 x 220.98 mm^3) with a 0.9 in (22.86 mm) flange around the aperture, which allowed the lens to be directly attached to the horn with bolts (see Figure 3(a)). The designed lens dimensions are 12.55 x 10.85 x 6.6 in^3 (318.77 x 275.59 x 167.64 mm^3). The second modification reduced the complexity of the GRIN by discretizing it into six symmetric layers, each being 1.1 in (27.94 mm) thick. Figure 3(b) shows how the top three layers mirror the bottom three layers, and each layer has 3 x 3 different regions mirrored twice to create a
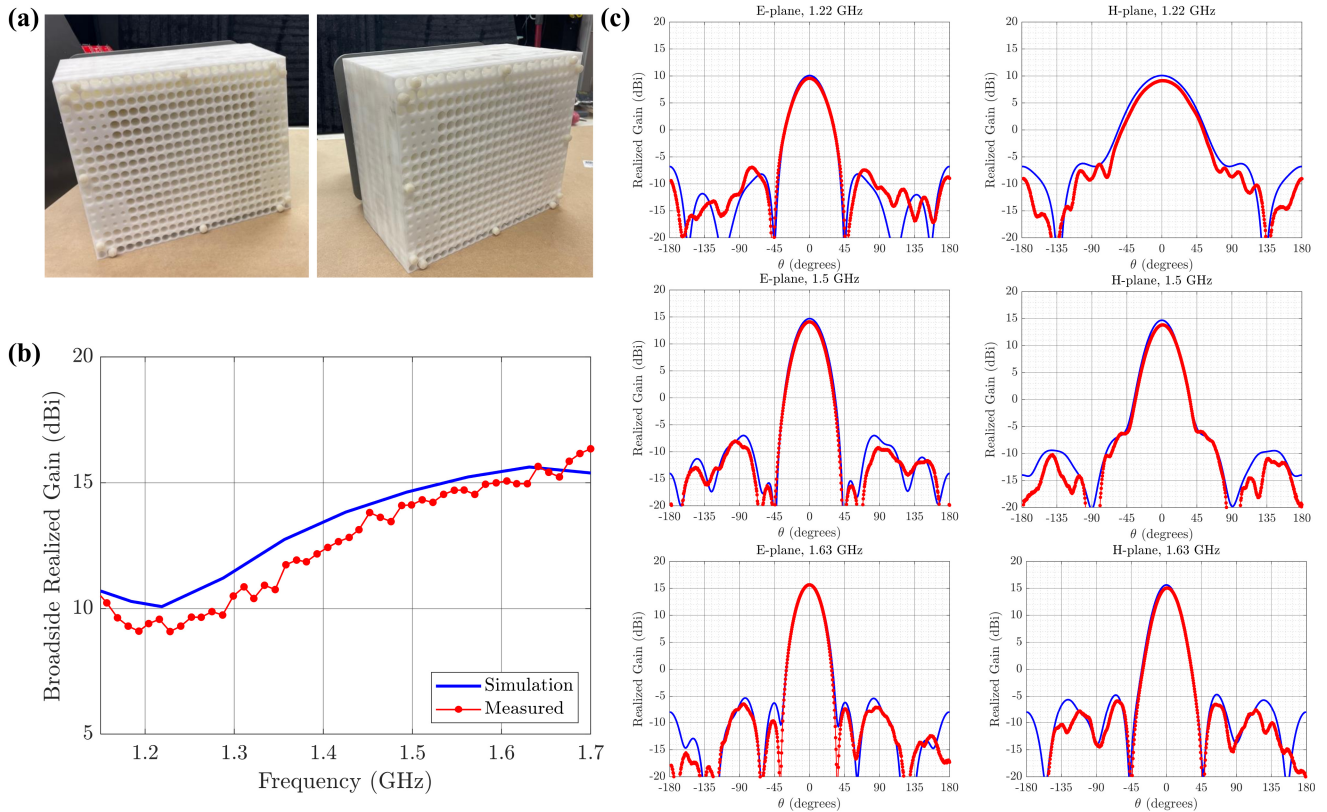
FIGURE 4. (a) Photos of the fabricated lens. (b) A comparison between the simulated and measured broadside realized gain for the lens- horn structure. (c) The E- and H-plane simulated and measured results for 1.22, 1.50, and 1.63 GHz. The 3 dB fractional bandwidth is 29% for the simulated design and 27% for the measured design.

two-fold symmetric structure. Holes of varying sizes were drilled into the Delrin 150 White material ($\epsilon_r = 3.1$, tan $\delta = 0.03$) along one axis to achieve the different permittivity values by varying the volume filling fraction of the combined dielectric/free-space media. These materials and production strategies made the lens easier and more affordable to fabricate with the final design being robust enough to support pressurization if required (a simple solid dielectric covering could be added to the design to fully enclose it). The final fabricated lens is displayed in Figure 4(a), which is seen to have similar size dimensions to the lens optimized in Section II-A.

The newly fabricated lens was reoptimized for maximum gain, lower side lobe levels and a symmetric beamwidth in the E- and H-planes. A symmetric beam pattern is important for attaining uniform illumination in the two orthogonal cuts and for maximizing aperture efficiency. Figure 4(b) shows that the realized gain of the fabricated lens agrees well with simulations from 1.2 to 1.7 GHz (the lens was designed for an operational frequency of 1.5 GHz), which confirms the efficacy of the chosen fabrication strategy. As further confirmation, Figure 4(c) shows the E- and H-plane realized gain patterns at 1.22, 1.50, and 1.63 GHz. The simulated and measured patterns show good agreement, which further validates our approach.

Lastly, we compare the fabricated lens design to the corresponding SGH. Figure 5 shows the realized gain pattern

in the E- and H-plane for (a) the SGH and (b) the fabricated lens design. The SGH has a peak gain of 16.8 dBi, while the fabricated lens has a peak gain of 14.7 dBi. We note that the peak gain levels are not as crucial for RA antennas since the overall system gain is mainly determined by the RA's size. Further, a higher gain horn needs to be placed farther from the RA, which increases the overall system size. In addition, our fabricated design has lower side lobes that are at least 21 dB below the main beam. On the other hand, the SGH has side lobes that are 14 dB below the main beam. Both designs have symmetric patterns in the E- and H-planes. This suggests that the fabricated design should have lower spillover than the SGH at a considerably smaller size. The area of the aperture and height of the fabricated lens is 50% and 48% less than that of the SGH, respectively. Thus, we were able to accurately fabricate a lens which could serve as a more compact feed for a RA antenna.

III. APERTURE EFFICIENCY IMPROVING GRIN FEEDS
A second avenue of this research is to explore GRIN lens designs that yield greater aperture efficiency and support higher power handling capability. Traditional feeds such as horns have a gradual taper where the feed location has to be optimized to balance spillover and illumination efficiency. The ideal radiation pattern would have no spillover and illuminate the aperture uniformly. However, standard feeds do not have these properties. Rather, the beam intensity usually
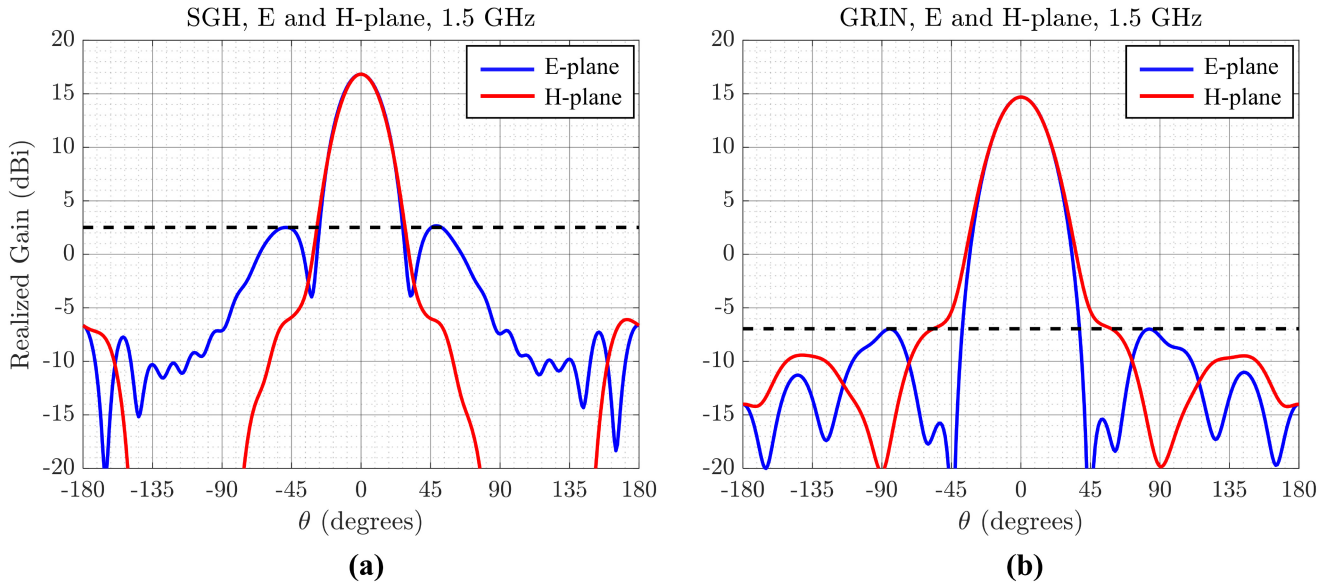
FIGURE 5. (a) The simulated realized gain pattern for standard gain horn (SGH). As can be seen the sidelobes are present around -14 dB down from the main beam. (b) The simulated realized gain patterns for the fabricated GRIN lens demonstrating that the total gain is comparable but with a marked decrease in the sidelobes levels while also achieving a reduction in the total occupying volume.

starts high at the center and then tapers towards the edge with significant spillover. Furthermore, to reduce blockage the feed often needs to be offset from the center of the reflector. This results in an asymmetric pattern, which makes finding the best feed source for a particular application even more challenging.

GRIN lenses provide a considerable ability to control the radiation coming from the source and can be used to improve the total aperture efficiency. However, what perhaps is more interesting is their ability to evenly distribute the power over the RA surface. In order to maximize power delivered to a location, either the gain or feed power level can be increased. Improving the gain can be achieved easily by simply increasing the size of the RA. However, this is undesirable, especially at low frequencies, since the RA can quickly become too large for many practical applications. Therefore, increasing the power levels is the better alternative. Yet this can easily lead power levels incident on the reflector that many RA antennas can no longer survive [37], [38], [39]. Even for more conservative power levels, power handling improvement could be valuable for electrically reconfigurable designs (*e.g.*, using varactordiodes) to prevent component failure. Therefore, improving aperture efficiency can improve gain and, hence, the amount of power delivered to a target. More evenly distributing the power across the reflectarray improves the power handling capability of the system.

A. COMPUTATIONAL METHODS

The aperture efficiency, η_{ap}, is calculated by multiplying the illumination and spillover efficiencies, which are obtained by integrating the fields over the surface where the RA would

be positioned (see [3]). The spillover efficiency η_{sp} is

$$\eta_{sp} = \frac{|\int_S P_z dS|}{P_{in}}, \qquad (1)$$

where S is the reflectarray surface to integrate over, P_z is the Poynting vector normal to the surface, and P_{in} is the total input power. Since the feed is pointed in the negative direction, we take the absolute value of the integration of the Poynting vector to remove the negative sign. The illumination efficiency η_{il} can be computed using:

$$\eta_{il} = \frac{\left(\int_S |E| dS\right)^2}{A \int_S |E|^2 dS}, \qquad (2)$$

where $|E|$ is the magnitude of the electric field, and A is the area of the RA. We note that this approach is slightly different than approaches based on far-field radiation patterns but is easier to compute for rectangular RAs.

Besides aperture efficiency, we also computed two other metrics in our analysis of the GRIN lens fed antenna systems. The first metric, K, is the peak electric field relative to the no-lens case

$$K = \max_S |E_{\text{NoGRIN}}| / \max_S |E_{\text{GRIN}}|, \qquad (3)$$

where E_{NoGRIN} and E_{GRIN} are the electric fields across the hypothetical reflectarray surface without and with the GRIN lens, respectively, for which we find the max value across the surface, S. This metric is very important when considering the power handling capability of the reflectarray since the location with the largest electric field will correspond to the most likely location for electrical breakdown. Therefore, minimizing the relative peak electric field is one of the main design objectives.
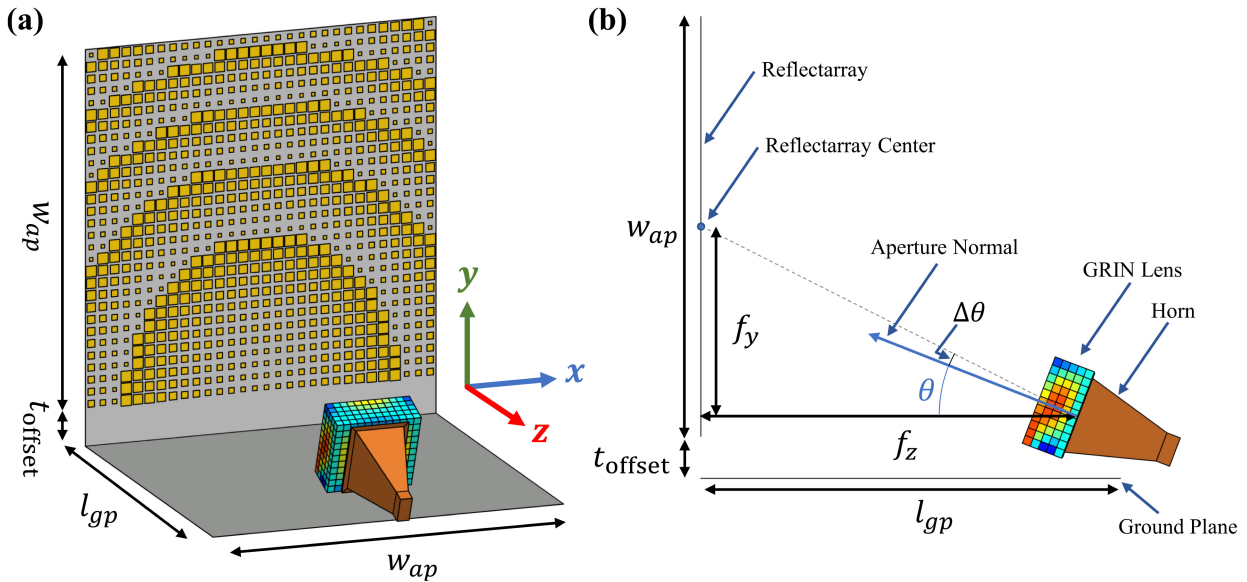
FIGURE 6. The RA setup. (a) A perspective profile with a ground plane beneath the feed horn and RA. (b) A side perspective with the horn pointing slightly below the center of the RA.

The second metric of interest is similar to illumination efficiency but better corresponds to characterizing a uniform field distribution. Here the proposed metric is

$$\eta_u = \frac{\underset{S}{\text{mean}}|E|^2}{\underset{S}{\text{max}}|E|^2}, \quad (4)$$

where we compute what we call the uniformity efficiency, η_u, from the mean electric field over the peak field across the surface. As will be shown later, this metric corresponds to a more uniform distribution of the electric field and therefore can be optimized to find designs that are better for handling high power levels. Illumination efficiency has the fault that it averages out peak values so, as will be shown later, two GRIN lens designs may have very similar illumination efficiencies but drastically different uniformity efficiencies.

Lastly, we compute what we call the relative effective radiated power (RERP), which is the effective radiated power relative to the no-GRIN lens case.

$$\text{RERP} = \left(\frac{\eta_{ap_{\text{GRIN}}}}{\eta_{ap_{\text{NoGRIN}}}}\right) K^2 \quad (5)$$

This expression indicates that a higher aperture efficiency with the GRIN lens will improve the gain of the reflectarray and result in higher power delivered to the target direction. Similarly, if the GRIN lens reduces the peak electric field magnitude across the RA surface, one can increase the feed power to increase the effective radiated power delivered to the target direction. Alternatively, a higher K value provides the RA with a larger safety factor before dielectric breakdown would occur.

B. REFLECTARRAY SETUP AND NO GRIN PERFORMANCE

There are many ways to set up the feed and RA system. For this proof-of-concept study, a 1 m (10 wavelength) per side square aperture is illuminated by a commercial off the shelf (COTS) pyramidal horn. The horn dimensions a, *b*, and l are 188 mm, 137.2 mm, and 211.3 mm, respectively. The horn flange was 13.5 mm. A horizontal ground plane of the same width as the RA was placed under the horn feed and extends from the RA surface to the end of the horn (see Figure 6).

Initially, the horn's location and direction were varied in a FEKO simulation framework to find the optimal position/orientation to achieve maximum aperture efficiency. Then, a GRIN lens was placed in front of the horn and the permittivity profile was optimized to achieve maximum effective radiated power compared to the no-lens case. Figure 7 shows the aperture efficiency for the no-lens case when (a) the horn is pointed at the center of the reflectarray and (b) when the horn is pointed −4 degrees below the center. Figure 7(a) unsurprisingly shows that the center-fed configuration is the optimal design choice, providing the largest total aperture efficiency. However, this horn positioning would result in increased blockage. On the other hand, with an offset feed, similar aperture efficiency to that of the center-fed system is achieved when the horn is positioned at −0.450 m below the center of the RA and 0.9 m away from the RA. This performance is enabled by tilting the feed horn slightly down from the center of the RA. After finding the feed location corresponding to the greatest aperture efficiency of the no-lens system, the GRIN lens was optimized to maximize aperture efficiency and to better distribute the
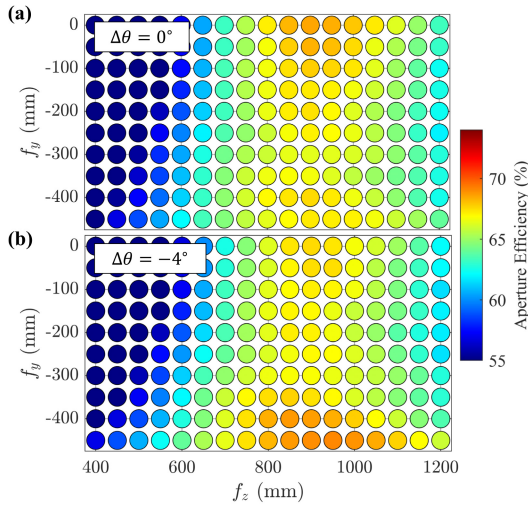
FIGURE 7. Computed aperture efficiency using the chosen horn antenna for different locations. (a) The horn pointed at the center of the reflector and (b) the horn pointed 4° below the center of the reflector. A similar aperture efficiency can be achieved with the horn offset from the center if its direction is slightly shifted, which could result in lower blockage.

power across the surface according to the metrics defined in Eqs. (1), (2), and (4).

C. OPTIMIZATION PROCEDURE

As pointed out in the introduction, several methods have been used to design GRIN lenses including transformation optics, field transformation methods, and ray tracing approaches. However, none of these methods have been used to tailor the fields on a RA surface. It is difficult to even know *a priori* what the optimal field pattern for the RA would even need to be since an ideal uniform field with zero spillover cannot be achieved in practice. Therefore, we used an optimization approach that would maximize the aperture efficiency and RERP instead of trying to target a specific near-field pattern on the RA. This technique is based on the GRIN lens generation method [40] but extended to support permittivity variations in all three orthogonal directions. The variables from the optimizer control the permittivity of a GRIN lens with a fixed size and position, while the objective function maximizes the RERP with the constraint that the aperture efficiency is greater than 65%. This constraint was necessary to prevent designs where there was high spillover, which would also result in a high K value (*i.e.*, since with high spillover there will also be less power incident on the RA).

To optimize the GRIN lens, we employed the CMA-ES algorithm to update the permittivity of 12 x 11 x 5 dielectric cubes that were each 2 cm on each side for a total lens size of 24 x 22 x 10 cm³. The GRIN profile was symmetric across the *yz*-plane. To efficiently optimize the permittivity of the lens, 18 control points were evenly distributed in a uniform 3 x 3 x 2 grid. The permittivity of each block was then found by performing a cubic interpolation between the control points. Since there were 660 different dielectric blocks, controlling the permittivity of each block would require too

many variables for global optimization. Thus, the interpolation scheme was necessary to reduce the number of variables down to 18. The angular tilt of the feed horn was also optimized. With this setup, we were able to create the design in CADFEKO using macros to build each of the dielectric blocks. The model was solved using the Multi-Level Fast Multipole Method (MLFMM) employing the surface equivalence principle setting in FEKO. The full-wave simulation of a GRIN lens, horn, and ground plane can be quite computationally expensive and would take 3-5 minutes per simulation on an Intel Xeon Gold 6258R with 56 cores and 1.5 TB of RAM. The optimizer ran 4765 different designs over the course of two weeks until the relative improvement from each iteration was negligible. Using this procedure, the optimizer found exemplary GRIN lens designs for this computationally intensive problem.

D. OPTIMIZATION RESULTS

Using the optimization procedure described, we were able to successfully find GRIN lenses that improved the aperture efficiency and power handling capability of the RA. Figures 8(a) and (b) show the set of best solutions that have varying amounts of illumination and spillover with the color bar indicating the aperture efficiency and RERP, respectively. Design 1, designated by the 5-pointed star, is the no-lens case, while all circles represent GRIN lens designs that have different amounts of improvement in illumination, spillover, or aperture efficiency. Design 2 corresponds to the design that was selected to be fabricated. It has the same aperture efficiency as the no-lens case but an improved power handling capability. This is a result of the more uniform distribution of the electric field across the surface of the RA, which can be seen by comparing the fields in subplots (1) and (2). We note that Design 2 has the same aperture efficiency but higher illumination and lower spillover efficiency than the no-lens case. Design 3, on the other hand, improves the aperture efficiency by maintaining both a better spillover and illumination efficiency than the no-lens case. However, this design does not distribute the electric field more uniformly across the RA and does not have better power handling capability than the no-lens design. Nevertheless, the RERP is slightly improved because of the increase in aperture efficiency. Lastly, Design 4 shows the design with maximum RERP. Here the aperture efficiency is very similar to the no-lens case, but like Design 2, the illumination efficiency is better while the spillover efficiency is lower. Even so, because of the more uniform distribution of the electric field across the surface, the design can handle higher power levels, which results in greater power delivered to the target direction. The computed efficiencies and metrics for the four different cases are provided in Table 1.

It seems logical to think that the illumination efficiency would provide a good objective for making the electric field more uniform. However, because this metric averages the field across the entire surface, the reported illumination efficiency can be high while the fields over the aperture
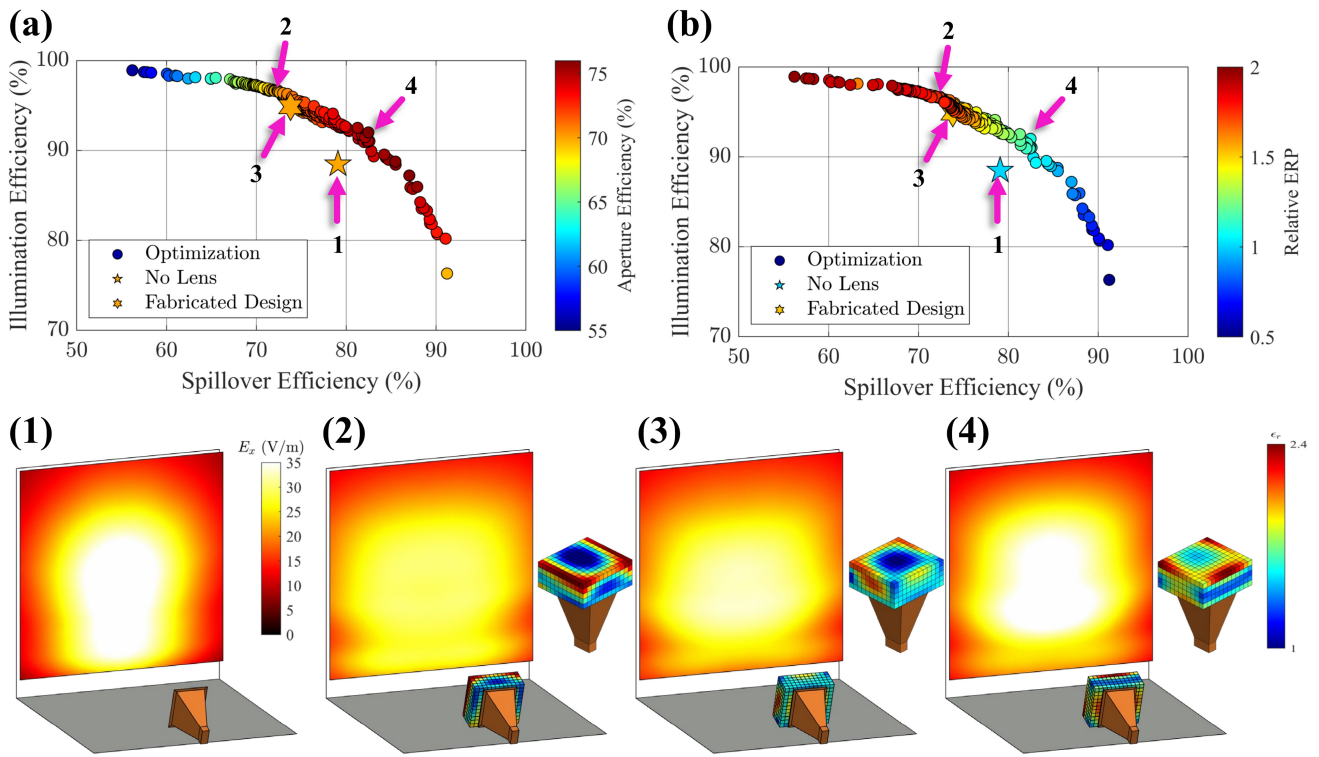
FIGURE 8. The set of best designs found from the optimization showing the spillover and illumination efficiency. The colorbar indicates the (a) aperture efficiency and (b) the RERP. Across the bottom is shown the electric field magnitude for each of the selected designs indicated in subplots (a) and (b) as well as the GRIN lens for designs (2)–(4).
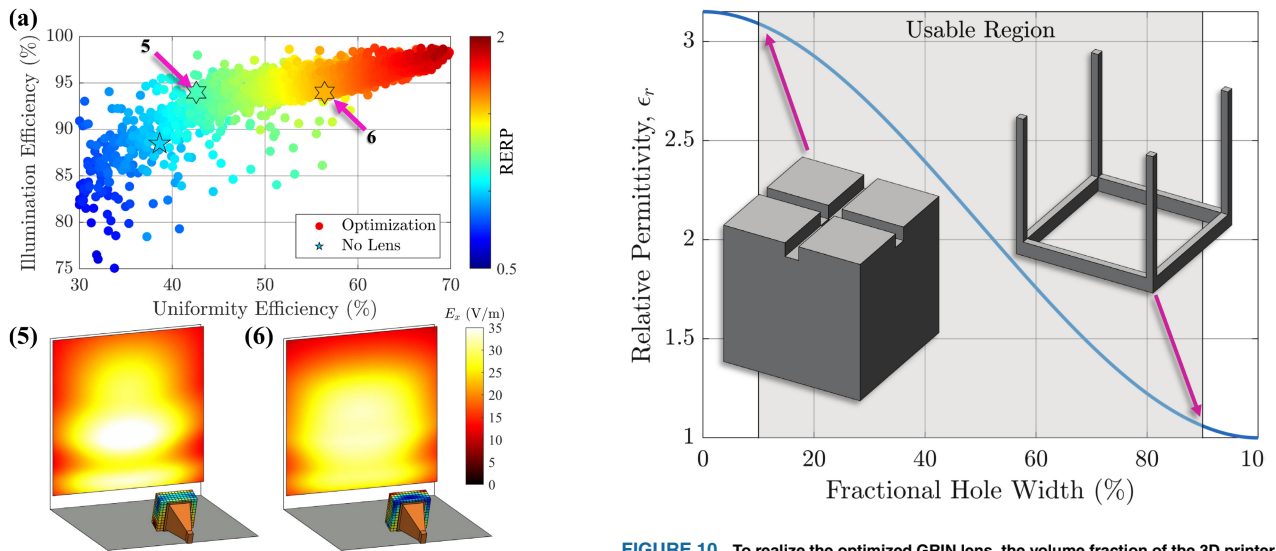

FIGURE 9. (a) The illumination and uniformity efficiency metrics for the designs simulated during the optimization. Designs (5) and (6) have similar illumination efficiency, but Design (6) has a better uniformity of the electric field as can be seen in the subplots.

FIGURE 10. To realize the optimized GRIN lens, the volume fraction of the 3D printer material to air ratio is adjusted to achieve an effective relative permittivity between 1.1 and 3.1. The unit cell design is shown as an inset. By composing the different unit cells together, the entire GRIN lens with inhomogeneous permittivity can be realized.

still possess hotspots, thereby degrading the overall system performance. Instead, an alternative objective measuring field uniformity was devised and included in the optimization objectives. Figure 9(a) shows the illumination and uniformity efficiencies for designs simulated during the optimization. Clearly, there is a positive correlation between these two
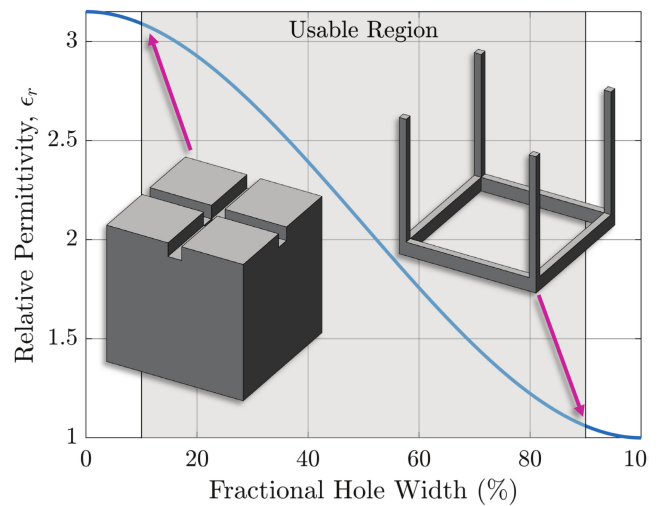
metrics. However, to demonstrate the differences between the two efficiencies, we picked two designs, Designs 5 and 6, with similar illumination and aperture efficiency, but differing uniformity efficiency. The field plots in Figure 9 show that Design 6 exhibits a lower peak electric field than that of Design 5. This peak field reduction makes Design 6 more suitable for handling high power and for corresponding applications.
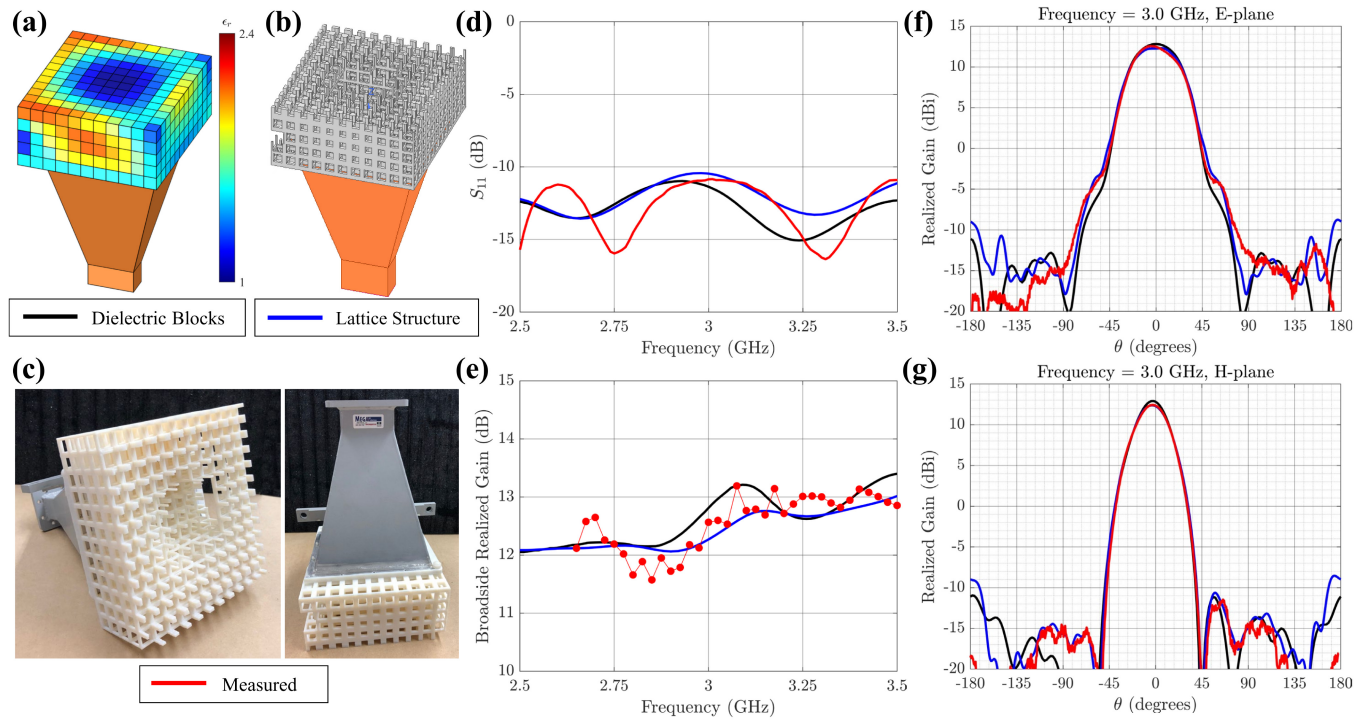
FIGURE 11. (a) The GRIN lens was simulated as discrete blocks of varying permittivity in FEKO. (b) The varying permittivity was used to compute the size of the hole in the dielectric material to form the entire 3D printable lens, which was then simulated in HFSS. (c) The GRIN lens was 3D printed using a Stratasys Object printer and attached to the commercially available horn. The (d) S_{11}, (e) realized gain, (f) E-plane gain pattern, and (g) H-plane gain pattern for the two simulated models as well as the measured GRIN lens and horn. The 3 dB fractional bandwidth for all three designs is 33%, the same as that of the feed horn.

TABLE 1. The simulated efficiencies for the selected feed designs.

Efficiency	(1) No Lens	(2) Fabricated	(3) Max Aperture Efficiency	(4) Max ERP
η_{ap} (%)	70.0	70.0	75.9	70.3
η_{sp} (%)	79.1	73.8	82.5	73.3
η_{il} (%)	88.5	94.9	92.0	96.0
η_{u} (%)	38.7	53.5	40.7	64.6
K	1	1.21	1.00	1.34
$RERP$	1	1.47	1.08	1.81

E. FABRICATION AND CHARACTERIZATION

To demonstrate that the GRIN lens works according to the simulations, we fabricated the selected design and measured the corresponding radiation pattern of the synthesized feed in an anechoic chamber. A design was selected based on similar aperture efficiency to that of the no-lens case and maximum field handling capability as well as ease of fabrication. The permittivity of each block was used to determine (based on Figure 10) the ratio of 3D printer material to air needed. Using an automated script, the structure was built in Ansys High Frequency Simulation Software (HFSS) and the result was exported as an STL file. We then used a Stratasys Object260 Connex3 printer which uses a VeroWhitePlus material with a permittivity of approximately 3.15 at 3 GHz and a loss tangent of 0.02. We performed a simulation where the permittivity was changed to 3 and found only

minor deviations in the radiation pattern. The GRIN lens was printed with support material that then had to be cleaned away. To maintain structural integrity, the minimum feature size for the 3D printer or holes was restricted to be greater than 4 mm. The unit cell was designed to be thicker on the bottom to give better support for attaching the lens to the horn. However, the lens' weight and size slightly warped it as it was printed, which resulted in a slight curvature of the lens. Nevertheless, this did not change the performance significantly.

The fabricated lens was measured in an anechoic chamber. Figures 11(a) and (b) show the FEKO and HFSS models, with the HFSS model using the 3D printed lattice. Figure 11(c) shows photographs of the fabricated lens with the horn antenna attached. The simulation as well as the measured results of the two models are provided in Figures 11(d)-(g). Figure 11(d) shows that the S_{11} is below -10 dB from 2.5 to 3.5 GHz for both the two simulation models and the fabricated design. Figure 11(e) shows that the broadside realized gain agrees well between the simulations and the measured data. Figures 11(f) and (g) show the radiation pattern of the lens and horn feed system at 3 GHz in the E- and H-plane, respectively. We see that there is very good agreement between the simulations and measurement indicating that the lens will perform as expected.

IV. CONCLUSION

There is a current need for RA antenna systems capable of handling high-power radiation in a condensed size. This

requires feeds that have high gain but are more compact, reducing the overall size of the system and minimizing blockage caused by the feed. Applications involving the real-world deployment of high-power systems may have space constraints, which means the ERP cannot be improved simply by increasing the aperture size and thereby the system gain. Alternatively, this necessitates that the feed more evenly spread out the energy to achieve a higher aperture efficiency and to prevent "hotspots" from being formed that could damage the RA unit cells. While previous approaches for designing feeds have focused on different kinds of metallic radiators, this work demonstrated methods for optimizing GRIN lenses that can better tailor the fields across the reflector. We designed and fabricated GRIN lenses with horn antennas that have high gain, but in a much more compact size and smaller aperture than a conventional standard gain horn. In addition, this work showed that GRIN lenses can be optimized to achieve higher aperture efficiency while more uniformly distributing the energy across the reflector surface to minimize electric field hotspots. GRIN lenses offer greater control over the radiation from a feed and can thereby significantly improve the performance of reflectors resulting in smaller and more powerful RA and TA systems.

REFERENCES

[1] J. Huang and J. A. Encinar, *Reflectarray Antennas*. Hoboken, NJ, USA: Wiley, 2008.

[2] J. Shaker, M. R. Chaharmir, and J. Ethier, *Reflectarray Antennas: Analysis, Design, Fabrication, and Measurement*. Boston, MA, USA: Artech House, 2014.

[3] A. Yu, F. Yang, A. Z. Elsherbeni, J. Huang, and Y. Rahmat-Samii, "Aperture efficiency analysis of reflectarray antennas," *Microw. Opt. Technol. Lett.*, vol. 52, pp. 364–372, Feb. 2010.

[4] P. J. B. Clarricoats and G. T. Poulton, "High-efficiency microwave reflector antennas—A review," *Proc. IEEE*, vol. 65, no. 10, pp. 1470–1504, Oct. 1977.

[5] A. D. Olver, P. J. B. Clarricoats, A. A. Kishk, and L. Shafai, *Microwave Horns and Feeds*. New York, NY, USA: Inst. Electr. Electron. Eng., 1994.

[6] E. Lier, D. H. Werner, and T. S. Bird, "The evolution from metal horns to metahorns: The development of EM horns from their inception to the present day," *IEEE Antennas Propag. Mag.*, vol. 61, no. 4, pp. 6–18, Aug. 2019.

[7] P. D. Potter, "A new horn antenna with suppressed sidelobes and equal beamwidths," *Microw. J.*, vol. 6, pp. 71–78, Feb. 1963.

[8] A. K. Bhattacharyya and G. Goyette, "A novel horn radiator with high aperture efficiency and low cross-polarization and applications in arrays and multibeam reflector antennas," *IEEE Trans. Antennas Propag.*, vol. 52, no. 11, pp. 2850–2859, Nov. 2004.

[9] P. J. B. Clarricoats and A. D. Olver, *Corrugated Horns for Microwave Antennas*. London, U.K.: Peter Peregrinus Ltd., 1984.

[10] B. Thomas, "Design of corrugated conical horns," *IEEE Trans. Antennas Propag.*, vol. AP-26, no. 2, pp. 367–372, Mar. 1978.

[11] L. Oh, S. Peng, and C. Lunden, "Effects of dielectrics on the radiation patterns of an electromagnetic horn," *IEEE Trans. Antennas Propag.*, vol. AP-18, no. 4, pp. 553–556, Jul. 1970.

[12] G. Tsandoulas and W. Fitzgerald, "Aperture efficiency enhancement in dielectrically loaded horns," *IEEE Trans. Antennas Propag.*, vol. AP-20, no. 1, pp. 69–74, Jan. 1972.

[13] E. Lier and P.-S. Kildal, "Soft and hard horn antennas," *IEEE Trans. Antennas Propag.*, vol. 36, no. 8, pp. 1152–1157, Aug. 1988.

[14] A. D. Olver and A. A. Saleeb, "Improved radiation characteristics of conical horns with plastics-foam lenses," *IEE Proc. H, Microw. Opt. Antennas*, vol. 130, no. 3, pp. 197–202, 1983.

[15] X. Chen, H. F. Ma, X. Y. Zou, W. X. Jiang, and T. J. Cui, "Three-dimensional broadband and high-directivity lens antenna made of metamaterials," *J. Appl. Phys.*, vol. 110, no. 4, pp. 1–8, Aug. 2011.

[16] E. B. Whiting et al., "Adjoint sensitivity optimization of three-dimensional directivity-enhancing, size-reducing GRIN lenses," *IEEE Antennas Wireless Propag. Lett.*, vol. 21, pp. 2166–2170, 2022.

[17] G. Oliveri, E. T. Bekele, M. Salucci, and A. Massa, "Transformation electromagnetics miniaturization of sectoral and conical metamaterial-enhanced horn antennas," *IEEE Trans. Antennas Propag.*, vol. 64, no. 4, pp. 1508–1513, Apr. 2016.

[18] K. V. Hoel, M. Ignatenko, S. Kristoffersen, E. Lier, and D. S. Filipovic, "3-D printed monolithic GRIN dielectric-loaded double-ridged horn antennas," *IEEE Trans. Antennas Propag.*, vol. 68, no. 1, pp. 533–539, Jan. 2020.

[19] F.-Y. Meng et al., "Automatic design of broadband gradient index metamaterial lens for gain enhancement of circularly polarized antennas," *Progr. Electromagn. Res.*, vol. 141, pp. 17–32, Jul. 2013.

[20] S. Shahcheraghi and A. Yahaghi, "Design of a pyramidal horn antenna with low E-plane sidelobes using transformation optics," *Progr. Electromagn. Res. M*, vol. 44, pp. 109–118, Oct. 2015.

[21] J.-M. Poyanco, F. Pizarro, and E. Rajo-Iglesias, "3D-printing for transformation optics in electromagnetic high-frequency lens applications," *Materials*, vol. 13, no. 12, p. 2700, Jun. 2020.

[22] H. F. Ma and T. J. Cui, "Three-dimensional broadband and broad-angle transformation-optics lens," *Nat. Commun.*, vol. 1, no. 1, p. 124, Dec. 2010.

[23] Z. L. Mei, J. Bai, and T. J. Cui, "Gradient index metamaterials realized by drilling hole arrays," *J. Phys. D, Appl. Phys.*, vol. 43, no. 5, Feb. 2010, Art. no. 55404.

[24] D.-H. Kwon and D. H. Werner, "Transformation electromagnetics: An overview of the theory and applications," *IEEE Antennas Propag. Mag.*, vol. 52, no. 1, pp. 24–46, Feb. 2010.

[25] D. H. Werner and D.-H. Kwon, Eds., *Transformation Electromagnetics and Metamaterials: Fundamental Principles and Applications*. London, U.K.: Springer, 2014.

[26] C. Mateo-Segura, A. Dyke, H. Dyke, S. Haq, and Y. Hao, "Flat Luneburg lens via transformation optics for directive antenna applications," *IEEE Trans. Antennas Propag.*, vol. 62, no. 4, pp. 1945–1953, Apr. 2014.

[27] S. Jain, M. Abdel-Mageed, and R. Mittra, "Flat-lens design using field transformation and its comparison with those based on transformation optics and ray optics," *IEEE Antennas Wireless Propag. Lett.*, vol. 12, pp. 777–780, 2013.

[28] E.-S. Jo and D. Kim, "3-D printer based lens design method for integrated lens antennas," *IEEE Antennas Wireless Propag. Lett.*, vol. 17, pp. 2090–2093, 2018.

[29] N. Zhang, W. X. Jiang, H. F. Ma, W. X. Tang, and T. J. Cui, "Compact high-performance lens antenna based on impedance-matching gradient-index metamaterials," *IEEE Trans. Antennas Propag.*, vol. 67, no. 2, pp. 1323–1328, Feb. 2019.

[30] M. Q. Qi et al., "Suppressing side-lobe radiations of horn antenna by loading metamaterial lens," *Sci. Rep.*, vol. 5, p. 9113, Aug. 2015.

[31] Y. Cao and S. Yan, "A low-profile high-gain multi-beam antenna based on 3D-printed cylindrical Luneburg lens," *Microw. Opt. Technol. Lett.*, vol. 63, no. 7, pp. 1965–1971, Jul. 2021.

[32] O. Quevedo-Teruel, J. Miao, M. Mattsson, A. Algaba-Brazalez, M. Johansson, and L. Manholm, "Glide-symmetric fully metallic Luneburg lens for 5G communications at Ka-band," *IEEE Antennas Wireless Propag. Lett.*, vol. 17, pp. 1588–1592, 2018.

[33] Y. Su and Z. N. Chen, "A flat dual-polarized transformation-optics beamscanning Luneburg lens antenna using PCB-stacked gradient index metamaterials," *IEEE Trans. Antennas Propag.*, vol. 66, no. 10, pp. 5088–5097, Oct. 2018.

[34] J. Budhu and Y. Rahmat-Samii, "A novel and systematic approach to inhomogeneous dielectric lens design based on curved ray geometrical optics and particle swarm optimization," *IEEE Trans. Antennas Propag.*, vol. 67, no. 6, pp. 3657–3669, Jun. 2019.

[35] "PREPERM-standard-grade-selection-102020.pdf." Accessed: Oct. 7, 2020. [Online]. Available: https://www.preperm.com/wp-content/uploads/2020/10/PREPERM-Standard-Grade-Selection-102020.pdf

[36] M. Sporer, R. Weigel, and A. Koelpin, "A 24 GHz dual-polarized and robust dielectric rod antenna," *IEEE Trans. Antennas Propag.*, vol. 65, no. 12, pp. 6952–6959, Dec. 2017.

[37] M. D. Gregory et al., "High power metasurface reflectarray antennas using switched shorted circular elements," in *Proc. IEEE Int. Symp. Antennas Propag. USNC/URSI Nat. Radio Sci. Meeting*, San Diego, CA, USA, Jul. 2017, pp. 1037–1038.

[38] M. D. Gregory et al., "Metamaterials for high power reflectarray design," in *Proc. IEEE/ACES Int. Conf. Wireless Inf. Technol. Syst. (ICWITS) Appl. Comput. Electromagn. (ACES)*, Honolulu, HI, USA, Mar. 2016, pp. 1–2.

[39] S. D. Campbell et al., "Metamaterial-enabled reflectarray antennas for high-power microwave applications," in *Proc. IEEE Int. Symp. Antennas Propag. North Amer. Radio Sci. Meeting*, Montreal, QC, Canada, Jul. 2020, pp. 651–652.

[40] J. Xu et al., "Multiobjective optimization of bespoke gradient-index lenses: A powerful tool for overcoming the limitations of transformation optics," *Phys. Rev. Appl.*, vol. 18, no. 2, pp. 1–9, Aug. 2022.
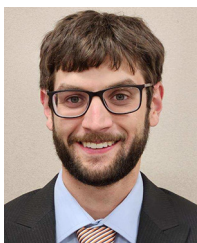
COLIN A. MUSSMAN (Graduate Student Member, IEEE) received the B.S. degree in electrical engineering from Virginia Polytechnic Institute and State University (Virginia Tech), Blacksburg, VA, USA, in 2016. He is currently pursuing the Ph.D. degree in electrical engineering with the Computational Electromagnetics and Antennas Research Laboratory, The Pennsylvania State University (Penn State), University Park, PA, USA, under the guidance of Dr. D. Werner. From 2016 to 2019, he worked as an Electronics Engineer with Naval Research Laboratory, Washington, DC, USA, in the Advanced Space Positioning, Navigation, and Timing branch. His current research interests include antenna design, ultrawideband phased arrays, high power microwave antennas, and metamaterials.

ERIC B. WHITING (Member, IEEE) received the B.S. degree in electrical engineering and the M.S. degree in physics from Brigham Young University in 2014 and 2016, respectively, and the Ph.D. degree in electrical engineering from The Pennsylvania State University in 2022. His research interests include metasurface and gradient index lens design.

SAWYER D. CAMPBELL (Senior Member, IEEE) received the B.S. degree in physics from Illinois Wesleyan University, Bloomington, IL, USA, in 2008, and the M.S. and Ph.D. degrees in optical sciences from The University of Arizona, Tucson, AZ, USA, in 2010 and 2013, respectively. He was an Undergraduate Researcher with the Intense Laser Physics Theory Unit, Department of Physics, Illinois State University from 2004 to 2008. He was then a Graduate Research Associate with the La Casa de Creative Electromagneticists, Department of Electrical and Computer Engineering, University of Arizona, under the advisement of Prof. R. W. Ziolkowski. In 2014, he joined the Computational Electromagnetics and Antennas Research Laboratory, Department of Electrical Engineering, The Pennsylvania State University as a Postdoctoral Scholar under the advisement of Prof. D. H. Werner. Since 2022, he has been an Associate Research Professor with the Department of Electrical Engineering, Penn State University and an Associate Director of the Computational Electromagnetics and Antennas Research Laboratory. He has extensive experience in the computational modeling and inverse-design of metamaterial- and transformation optics-based devices at RF, infrared, and optical frequencies. Additionally, he is an expert in the application of multiobjective and surrogate-assisted optimization techniques to challenging problems in both the RF and optical regimes. He has published over 150 technical papers and proceedings articles, a book on nanoantennas and plasmonics, and is the author/coauthor of five book chapters. His current research interests include metasurfaces, nanophotonics, gradient-index lenses, high power microwave antennas, optimization, and applications of deep learning to RF, and optical inverse-design problems. He is a Senior Member of the OPTICA and SPIE and is the Past Chair and the Current Vice-Chair/Treasurer of the IEEE Central Pennsylvania Section.

GALESTAN MACKERTICH-SENGERDY (Member, IEEE) received the B.S. degree in mechanical engineering and the M.S. degree in engineering science and mechanics from Penn State University, University Park, PA, USA, where he is currently pursuing the Ph.D. degree in electrical engineering. From 2009 to 2018, he worked in industry as a Mechanical Engineer. Since 2019, he has been a Researcher with the Computational Electromagnetics and Antennas Research Laboratory, Penn State University. His research interests include designing mechanically robust, high-power, and metamaterial antenna systems.

RYAN J. CHAKY (Graduate Student Member, IEEE) received the B.S. degree in electrical engineering from Bucknell University, Lewisburg, PA, USA, in 2017. He is currently pursuing the Ph.D. degree with The Pennsylvania State University as a member of the Computational Electromagnetics and Antennas Research Laboratory. His research interests currently include reflectarrays, transmitarrays, RCS reduction and cloaking, reflector systems, GRIN lenses, metamaterial and metasurface design and optimization, plasmonic antennas, nanoantennas, electromagnetic theory, reconfigurable antennas, and computational electromagnetics.

PINGJUAN L. WERNER (Life Senior Member, IEEE) received the Ph.D. degree in electrical engineering from The Pennsylvania State University, USA, in 1991. She is a Distinguished Professor with the Pennsylvania State University College of Engineering. Her primary research focuses are in the area of electromagnetics, including fractal antenna engineering, and the application of genetic algorithms in electromagnetics. She received The Best Paper Award from the Applied Computational Electromagnetics Society in 1993. She is a Fellow of the Leonhard Center, College of Engineering, The Pennsylvania State University and a member of Tau Beta Pi National Engineering Honor Society, Eta Kappa Nu National Electrical Engineering Honor Society, Sigma Xi National Research Honor Society.

DOUGLAS H. WERNER (Fellow, IEEE) received the B.S., M.S., and Ph.D. degrees in electrical engineering and the M.A. degree in mathematics from the Pennsylvania State University (Penn State), University Park, in 1983, 1985, 1989, and 1986, respectively.

He holds the John L. and Genevieve H. McCain Chair Professorship with the Department of Electrical Engineering, The Pennsylvania State University. He is the Director of the Computational Electromagnetics and Antennas Research Lab as well as a Faculty Member with the Materials Research Institute, Penn State. He holds 20 patents, has published over 1000 technical papers and proceedings articles, and 30 book chapters with several additional chapters currently in preparation. He has published seven books, including *Frontiers in Electromagnetics* (Piscataway, NJ, USA: IEEE Press, 2000), *Genetic Algorithms in Electromagnetics* (Hoboken, NJ, USA: Wiley-IEEE Press, 2007), *Transformation Electromagnetics and Metamaterials: Fundamental Principles and Applications* (London, U.K.: Springer, 2014), *Electromagnetics of Body Area Networks: Antennas, Propagation, and RF Systems* (Hoboken, NJ, USA: Wiley/IEEE, 2016), *Broadband Metamaterials in Electromagnetics: Technology and Applications* (New York: Taylor and Francis Group, 2017), *Nanoantennas and Plasmonics: Modelling, Design and Fabrication* (London, U.K.: SciTech Publishing, IET, 2020), and *Electromagnetic Vortices: Wave Phenomena and Engineering Applications* (Hoboken, NJ, USA: Wiley-IEEE Press, 2021). He has also contributed chapters for several books, including *Electromagnetic Optimization by Genetic Algorithms* (New York: Wiley Interscience, 1999), *Soft Computing in Communications* (New York: Springer, 2004), *Antenna Engineering Handbook* (New York: McGraw-Hill, 2007), *Frontiers in Antennas: Next Generation Design and Engineering* (New York: McGraw-Hill, 2011), *Numerical Methods for Metamaterial Design* (New York: Springer, 2013), *Computational Electromagnetics* (New York: Springer, 2014), *Graphene Science Handbook: Nanostructure and Atomic Arrangement* (Abingdon, Oxfordshire, U.K.: CRC Press, 2016), *Handbook of Antenna Technologies* (New York: Springer, 2016), and *Transformation Wave Physics: Electromagnetics, Elastodynamics and Thermodynamics* (Boca Raton, FL, USA: CRC Press, 2016). His research interests include computational electromagnetics (MoM, FEM, FEBI, FDTD, DGTD, CBFM, RCWA, GO, and GTD/UTD) antenna theory and design, phased arrays (including ultra-wideband arrays), high-power microwave devices, wireless and personal communication systems (including on-body networks), wearable and e-textile antennas, RFID tag antennas, conformal antennas, reconfigurable antennas, frequency selective surfaces, electromagnetic wave interactions with complex media, metamaterials, electromagnetic bandgap materials, zero and negative index materials, transformation optics, nanoscale electromagnetics (including nanoantennas), fractal and knot electrodynamics, and nature-inspired optimization techniques (genetic algorithms, clonal selection algorithms, particle swarm, wind driven optimization, and various other evolutionary programming schemes).

Prof. Werner received the Pennsylvania State University Applied Research Laboratory Outstanding Publication Award in 1994. He was presented with the 1993 Applied Computational Electromagnetics Society Best Paper Award and was also the recipient of a 1993 International Union of Radio Science Young Scientist Award. He was a coauthor (with one of his graduate students) of a paper published in the IEEE TRANSACTIONS ON ANTENNAS AND PROPAGATION which received the 2006 R. W. P. King Award. He received the IEEE Antennas and Propagation Society Edward E. Altshuler Prize Paper Award and the *Harold A. Wheeler Applications Prize Paper Award* in 2011 and 2014, respectively. In 2018, he received the *DoD Ordnance Technology Consortium (DOTC) Outstanding Technical Achievement Award*. He also received the *2015 ACES Technical Achievement Award*, the *2019 ACES Computational Electromagnetics Award*, and the IEEE Antennas and Propagation Society 2019 Chen-To Tai Distinguished Educator Award. He was the recipient of a College of Engineering PSES Outstanding Research Award and Outstanding Teaching Award in March 2000 and March 2002, respectively. In March 2009, he received the PSES Premier Research Award. He was also presented with an IEEE Central Pennsylvania Section Millennium Medal. He is a former Associate Editor of *Radio Science*, a former Editor of the *IEEE Antennas and Propagation Magazine*, a former Editorial Board Member of *Scientific Reports* (a Nature subjournal), an Editorial Board Member for *EPJ Applied Metamaterials*, an Editor for the IEEE PRESS SERIES ON ELECTROMAGNETIC WAVE THEORY AND APPLICATIONS, a member of URSI Commissions B and G, Eta Kappa Nu, Tau Beta Pi, and Sigma Xi. He is a Fellow of IET, NAI, OPTICA, SPIE, ACES, and AAIA, and the PIER Electromagnetics Academy. He is also a Senior Member of the International Union of Radio Science.